ACS Catalysis

Research Article

Cite This: ACS Catal. 2019, 9, 2842−2853

pubs.acs.org/acscatalysis

Operando DRIFTS and DFT Study of Propane Dehydrogenation over Solid- and Liquid-Supported Ga_xPt_y Catalysts

Tanja Bauer,[†,▽] Sven Maisel,[‡,▽] Dominik Blaumeiser,[†] Julia Vecchietti,[§] Nicola Taccardi,[∥] Peter Wasserscheid,[∥,⊥,#] Adrian Bonivardi,[§] Andreas Görling,[‡] and Jörg Libuda*[,†,⊥]

[†]Lehrstuhl für Physikalische Chemie II, Friedrich-Alexander-Universität Erlangen-Nürnberg, Egerlandstraße 3, D-91058 Erlangen, Germany

[‡]Lehrstuhl für Theoretische Chemie, Friedrich-Alexander-Universität Erlangen-Nürnberg, Egerlandstraße 3, D-91058 Erlangen, Germany

[§]Instituto de Desarrollo Tecnológico para la Industria Química, Universidad Nacional del Litoral and CONICET, Güemes 3450, 3000 Santa Fe, Argentina

[∥]Lehrstuhl für Chemische Reaktionstechnik, Friedrich-Alexander-Universität Erlangen-Nürnberg, Egerlandstraße 3, D-91058 Erlangen, Germany

[⊥]Erlangen Catalysis Resource Center and Interdisciplinary Center for Interface-Controlled Processes, Friedrich-Alexander-Universität Erlangen-Nürnberg, 91058 Erlangen, Germany

[#]Forschungszentrum Jülich, "Helmholtz-Institute Erlangen-Nürnberg for Renewable Energies" (IEK 11), Egerlandstr. 3, 91058 Erlangen, Germany

Supporting Information

ABSTRACT: Supported catalytically active liquid metal solutions (SCALMS) represent a class of catalytic materials that have only recently been developed, but have already proven to be highly active, e.g., for dehydrogenation reactions. Previous studies attributed the catalytic activity to isolated noble metal atoms at the surface of a liquid and inert Ga matrix. In this study, we apply diffuse reflectance infrared Fourier transform spectroscopy (DRIFTS) with CO as a probe molecule to Ga/Al_2O_3, Pt/Al_2O_3, and $Ga_{37}Pt/Al_2O_3$ catalysts, to investigate in detail the nature of the active Pt species. Comparison of CO adsorption on Pt/Al_2O_3 and $Ga_{37}Pt/Al_2O_3$ shows that isolated Pt atoms are, indeed, present at the surface of the liquid SCALMS. Combining DRIFTS with online gas chromatography (GC), we investigated the Ga/Al_2O_3, Pt/Al_2O_3, and $Ga_{37}Pt/Al_2O_3$ systems under operando conditions during propane dehydrogenation in CO/propane and in Ar/propane. We find that the Pt/Al_2O_3 sample is rapidly poisoned by CO adsorption and coke, whereas propane dehydrogenation over $Ga_{37}Pt/Al_2O_3$ SCALMS leads to higher conversion with no indication of poisoning effects. We show under operando conditions that isolated Pt atoms are present at the surface of SCALMS during the dehydrogenation reaction. IR spectra and density-functional theory (DFT) suggest that both the Ga matrix and the presence of coadsorbates alter the electronic properties of the surface Pt species.

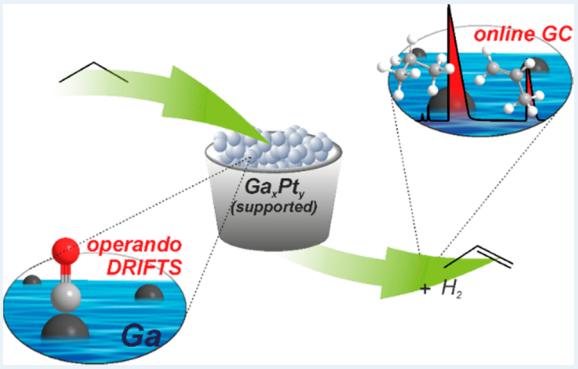

KEYWORDS: *SCALMS, dehydrogenation, DRIFTS, operando, DFT*

1. INTRODUCTION

The demand for light alkenes like ethylene, propene, and butene has increased in the past years, as they are widely employed as building blocks in a wide range of polymer and petrochemical production processes.[1−4] At the same time, the recent boom of natural gas production, e.g., from shale gas, increased the availability of C_2 to C_4 alkane raw materials.[1,5,6] Conventional methods to produce light olefins are steam cracking and fluid catalytic cracking (FCC) of naphtha, light diesel, and other crude oil distillation cuts.[1,2] Recently, alternative on-purpose routes have gained increasing industrial attention, in particular to meet the growing demand for propene.[7]

Catalytic dehydrogenation is a highly endothermic reaction, and at elevated temperatures side reactions such as cracking, hydrogenolysis, and isomerization are likely to occur.[3] The formation of byproducts and the resulting coke deposits leads to a decrease in catalyst selectivity and rapid catalyst deactivation.

Received: November 15, 2018
Revised: February 5, 2019
Published: February 15, 2019

DOI: 10.1021/acscatal.8b04578
ACS Catal. 2019, 9, 2842−2853

These are the main problems of typical dehydrogenation catalysts like Pt on alumina, CrO_x, or Ga_2O_3.[1,2,6,8]

To overcome these limitations, Taccardi et al. have recently developed a new type of dehydrogenation catalyst called supported catalytically active liquid metal solutions (SCALMS).[9] Low amounts of catalytically active noble metals, like Pd, are dissolved in Ga and supported on a porous support, like SiO_2 or Al_2O_3.[10] Ga is well-known to dissolve most transition metals and to form various intermetallic compounds (IMCs).[11−15] The catalytic activity of GaPd IMCs has been proven in previous studies, e.g., for hydrogenation of acetylene and methanol steam reforming.[11,16] The key difference of SCALMS to previous work on IMCs is that only very low amounts of noble metals are employed, which tremendously decreases the melting temperature of the system. Under dehydrogenation conditions (>350 °C) a homogeneous and liquid Ga/noble metal phase is present instead of a crystalline IMC. SCALMS perform with high selectivity and without coke formation in butane dehydrogenation.[9] It was proposed that isolated noble metal atoms on the surface of the inert, liquid Ga matrix act as catalytically active sites. Thus, SCALMS can be described as a new type of single-atom catalyst (SAC). The concept of site isolation has already been exploited e.g., like in Pt-containing single-atom alloys (SAAs) or PdZn alloys to efficiently suppress coke formation.[17,18] Moreover, it has been reported that application of PtCu SAAs strongly suppresses CO poisoning during the semihydrogenation of acetylene.[19]

This study presents a detailed characterization of a Pt-containing SCALMS and comparison with the respective Ga/Al_2O_3 and Pt/Al_2O_3 systems under operando conditions. We investigate the catalytically active Pt sites and determine how the noble metal is affected by the presence of a liquid Ga matrix. To that aim, we investigate Ga/Al_2O_3, Pt/Al_2O_3, and $Ga_{37}Pt$/Al_2O_3 during propane dehydrogenation using infrared (IR) spectroscopy with the use of CO as probe molecule. CO is well-known to adsorb on noble metals, and interpretation of its IR signature offers detailed insights into the coordination and electronic environment of the noble metal binding partner. Recently, SCALMS model systems were also prepared under ultrahigh vacuum (UHV) conditions, and the systems were characterized by IR spectroscopy of adsorbed CO.[20]

In the present work, we combine diffuse reflectance infrared Fourier transform spectroscopy (DRIFTS) and online gas chromatography (GC) measurements to correlate catalyst performance and the presence of surface sites during the dehydrogenation reaction. Density-functional theory (DFT)-based ab initio molecular dynamics (AIMD) simulations are used to investigate the surface composition of the catalyst and to assign the CO signals obtained. This approach helps in the understanding of the spectroscopic properties of CO adsorbed during propane dehydrogenation on SCALMS.

2. EXPERIMENTAL PROCEDURES, SETUPS, AND MATERIALS

2.1. Experimental Setup. The DRIFTS measurements were conducted using a high-temperature reactor chamber and Praying Mantis diffuse reflectance accessory (both from Harrick). The reactor chamber is equipped with CaF_2 windows and was modified with a type K thermocouple that measures the temperature directly in the catalyst powder. The reactor and DRIFTS accessory are placed in a home-built extension of a Bruker Vertex 80v spectrometer that provides all electrical and gas dosing feedthroughs required. This setup allows keeping the optical path and sample compartment evacuated during the experiment, leading to improved long-term stability. The spectrometer is equipped with a KBr beam splitter and a liquid N_2 HgCdTe detector. All spectra were recorded using an acquisition time of 1 min and 2 cm^{-1} spectral resolution. The pressure in the gas line system can be adjusted between 1 mbar and 20 bar using three pressure controllers (Bronkhorst) working in different pressure regimes. Five different gases can be dosed via mass flow controllers (Bronkhorst) using a flux between 0.2 and 20 mL_N/min.

The online GC measurements were performed using an Agilent 7890A GC with 1 mL sample loop (split ratio 5:1), a GS-GasPro capillary column (Agilent Technologies, length 30 m, inner diameter 0.32 mm), and a flame ionization detector (FID). The GC oven was constantly kept at 70 °C, which allows for sufficient separation of the signals.

The complete setup can be operated in a programmed and automatized way. This makes it possible to perform accurate and simultaneous changes in temperature, pressure, and gas composition and reproduce temperature profiles in a reliable way on different samples.

Ar (Linde, >99.999%) and propane (Linde, >99.5%) were used without further purification. CO (Linde, >99.997%) was passed through two consecutive carbonyl traps (catalytic trap from LPM and Gaskleen II Purifier from Pall Corporation) to ensure a Ni- and Fe-carbonyl-free gas feed.

The complete setup is depicted in the Supporting Information (Figure S1). It is optimized for the in situ and operando investigation of catalysts; however, trends concerning catalytic conversion and selectivity are in good agreement with reactor experiments, e.g., from a tubular fixed-bed reactor.

2.2. Experimental Procedure and Data Treatment. Three Ga_xPt_y/Al_2O_3 samples with varying Ga:Pt ratio and a pure Al_2O_3 sample were treated with the same experimental procedure described in this section. The composition of the samples, their Ga:Pt ratio, and expected melting temperature in the experiment are listed in Table 1.

Table 1. Composition of Examined Samples Obtained from ICP−AES and Expected Melting Temperatures

sample	metals	support	expected melting temperature
Al_2O_3		Al_2O_3	
Ga	7 wt % Ga	Al_2O_3	RT[a]
Pt	0.38 wt % Pt	Al_2O_3	
$Ga_{37}Pt_1$	8.9 wt % Ga, 0.67 wt % Pt (37:1 molar ratio)	Al_2O_3	270−330 °C[13,21]

[a]RT: room temperature.

Each sample was first reduced in 1 bar CO at 450 °C to remove the passivation layer present on the material. The DRIFTS background spectrum was recorded after cooling to 200 °C and removal of the CO gas phase in 1 bar Ar with an acquisition time of 10 min. The following procedure was performed in automatized mode. Each sample was probed during heating from 200 to 450 °C in steps of 50 °C and cooling back to 200 °C in the same fashion. At each temperature step, a sequence of five subsequent pulses of Ar/CO in propane was applied, each terminated by a short evacuation period. A scheme of the procedure is shown in Figure 1. At first, 10% Ar in propane was dosed for 19 min at 1 bar, followed by removal of the gas phase from the reactor in vacuo (~1 mbar) for 1 min. Second,

DOI: 10.1021/acscatal.8b04578
ACS Catal. 2019, 9, 2842−2853

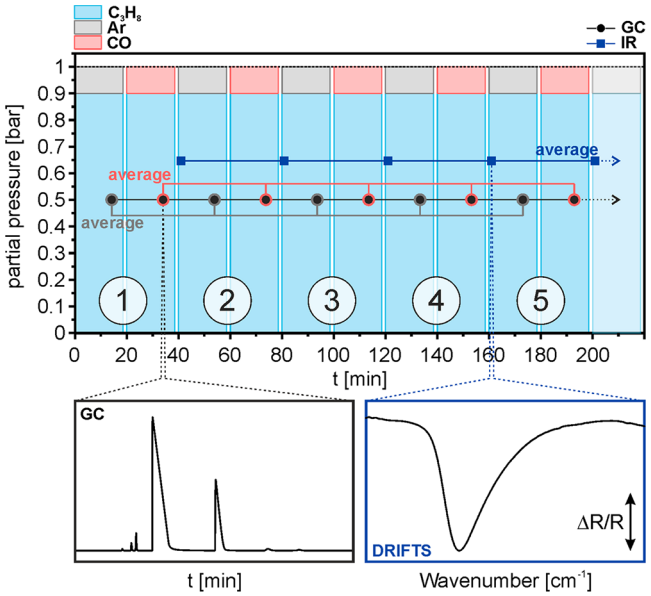

Figure 1. Schematic representation of the experimental procedure applied in the operando DRIFTS experiments.

CO in propane was dosed (10% CO, 19 min) and removed (evacuation to ~1 mbar for 1 min) in the same way. The sequence consisting of the two gas pulses and evacuation was repeated five times at each temperature (11 temperature steps in total).

For a study of the CO adsorption on the Pt-containing catalysts in the absence of propane, similar ramps were conducted with pure Ar and 10 vol % CO in Ar at 1 bar.

GC injections were performed 15 min after dosing of Ar/propane or CO/propane to evaluate the conversion of propane and the selectivity toward propene. Note that the calculated selectivity values obtained at low conversion are more prone to experimental errors and, therefore, not shown below. For details about the data evaluation, we refer to the Supporting Information.

DRIFTS spectra were constantly recorded during the procedure, but only selected ones are shown below. The procedure helps to characterize the metal surface sites with the help of CO as a probe molecule. The adsorbate signals are best seen in the absence of gas-phase CO, but a compromise has to be found between complete removal of CO from the gas phase and desorption of CO upon evacuation, especially at elevated temperatures. As indicated in Figure 1, all spectra presented were recorded immediately after removal of the CO/propane feed. The adsorbate signals are clearly visible in the spectra selected, but the spectra also show a noticeable CO gas-phase signal. The residual CO gas-phase signal was removed from the spectra using a suitable data treatment including a low pass filter.[22] For details we refer to the Supporting Information (Figure S2). The removal of the high-frequency rotational part of the CO gas-phase signal finally yields the spectra of adsorbed CO. The spectra were normalized to compensate for thermally induced changes in reflectivity (see Xu et al.[23]) and baseline-corrected.

2.3. Catalyst Preparation. All reactions requiring protective atmosphere were carried out using standard Schlenck techniques. All reagents were commercial and used as received. The Pt and Ga content of the catalyst samples, and their ratio, was determined by inductively coupled plasma−atom emission spectroscopy (ICP−AES) using a Ciros CCD instrument (Spectro Analytical Instruments GmbH). The solid samples were digested with concentrated HCl:HNO_3:HF in a 3:1:1 ratio in volume, using microwave heating up to 220 °C for 40 min. (CAUTION: HF solutions and vapors are extremely toxic, all manipulation has to be carried in a very efficient fume hood, wearing protective clothes, gloves, goggles.) The instrument was calibrated for Pt (241.423 nm) and Ga (417.206 nm) with standard solutions of the relevant elements prior to the measurements.

2.3.1. Preparation of Et_3NGaH_3. This compound was synthesized using a literature-described procedure[24] using triethylammonium chloride (Sigma-Aldrich) instead of trimethylammonium chloride. The compound was not isolated and used as ethereal solution. The Ga content of this solution was determined as follows: 1 mL of ethereal solution was quenched in 10 mL of HCl (~2 M), and the resulting mixture was shortly boiled to evaporate the diethyl ether. The homogeneous solution was then diluted to 500 mL and the Ga content determined by ICP−AES.

2.3.2. Preparation of Metallic Ga Decorated Alumina. A 100 g portion of neutral alumina (Sigma-Aldrich, mostly γ-alumina) was heated under vacuum (1 mbar) at 350 °C overnight in a 500 mL Schlenck flask. After the system was cooled, the material was suspended in 150 mL of dry diethyl ether, under argon. An ethereal solution of Et_3NGaH_3 was added to this suspension in such an amount to obtain the desired theoretical Ga loading (7−10% w/w of Ga) with respect to the support. The ether was removed under vacuum at ca. −30 °C. After complete removal of diethyl ether, the flask was quickly (ca. 10 °C/min) heated up to 300 °C and held at this temperature until no gaseous products were observed any longer. Et_3NGaH_3 thermally decomposes cleanly to metallic Ga, Et_3N, and H_2, and the volatile/gaseous components are completely removed in vacuum. Once the gallane decomposition terminated, the resulting gray solid was held at this temperature under vacuum (1 mbar) overnight and then cooled and stored under argon. The vapor pressure of the metallic Ga deposit is considered negligible under the conditions applied during the operando IR experiment (10^{-11} mbar at the highest operation temperatures in this work).[25] For further details on the experimental procedure see ref 9.

2.3.3. Preparation of Pt/Ga-Decorated Material. The deposition of Pt was obtained by partial galvanic displacement of metallic Ga by Pt^{2+}. To this purpose, 3 g of Ga/Al_2O_3 (9.8% w/w Ga) was suspended in 10 mL of distilled water under vigorous stirring. A 17.9 mL portion of a stock solution of $Pt(NO_3)_2$ (with a nominal Pt concentration of 1 mg/mL) in distilled water was added to this suspension. The resulting suspension was held under stirring for 15 min; then, the solid was filtered, and the material was thoroughly washed with distilled water (500 mL). The resulting solid was dried in an oven at 130 °C overnight. The structure of the $Ga_{37}Pt_1/Al_2O_3$ sample was investigated by SEM/EDX (see the SI for details). For a detailed investigation on structurally similar Pd−Ga systems, we refer to our previous publication.[9]

2.4. Computational Details. DFT calculations were carried out using the VASP code with periodic boundary conditions. The projector augmented wave (PAW) method was chosen together with a plane wave basis set.[26−28] Exchange-correlation effects were treated within the generalized gradient approximation (GGA) approach employing the Perdew−Burke−Ernzerhof (PBE) functional[29] in combination with the

DOI: 10.1021/acscatal.8b04578
ACS Catal. 2019, 9, 2842−2853

D3 correction of Grimme et al.[30] to investigate adsorption processes.

AIMD simulations were performed to characterize the GaPt catalyst and to study the CO adsorption behavior. Two approaches were tested and compared. First, a periodic surface slab model using a tetragonal unit cell (12.69 × 12.69 × 36.15 Å) containing 178 Ga and 2 Pt atoms, separated by at least 10 Å of vacuum to model the liquid−vacuum interface was generated in analogy to refs 9 and 31. Since liquid nanodroplets were previously observed in SCALMS experiments, we furthermore generated liquid GaPt nanoparticle (NP) models (Ga_{135}, $Ga_{132}Pt_3$, and $Ga_{125}Pt_{10}$) and compared the results to the slab system. The NPs were placed in a periodic box with at least 10 Å of vacuum in all spatial directions to decouple periodic images (see Figure S5). For systems with and without adsorbates, a kinetic energy cutoff for the plane wave basis of 450 and 300 eV was chosen, respectively. The equations of motion were integrated with a Verlet algorithm in time steps of 10 fs for surfaces/NPs without adsorbates, while for systems containing CO the time step was reduced to 2 fs. All systems were equilibrated for at least 5 ps before production runs were performed using a Nosé−Hoover thermostat[32] to simulate a canonical ensemble at 450 °C. A Fermi-smearing was chosen with a smearing width corresponding to the temperature conditions.[33] Γ-containing 2 × 2 × 1 *k*-point meshes were employed for the surface slab models, while for NPs only the Γ-point was sampled. Energy conservation during the AIMD run was ensured by an SCF convergence criterion of 10^{-7} eV. For an investigation of the Pt distribution in the liquid catalyst, three trajectories were simulated (each for at least 520 ps), and results were averaged. In general, for all mentioned AIMD simulations at least two independent trajectories were simulated to compare the results.

CO adsorption was studied by placing CO molecules at Pt sites located at the Ga surface in the beginning of the calculation. In the case of the slab approach one CO molecule with the corresponding Pt was located at each surface. In the NP model, three CO molecules were placed at the surface with large CO−CO separations. Subsequently, vibrational power spectra were computed using the trajectory analyzer code TRAVIS[34,35] by calculation of the Fourier transform of the velocity−velocity autocorrelation function. The power spectra of five trajectories were averaged, each running for 35 ps in the case of the slab approach. For the NP models, two trajectories were simulated (each with three adsorbed CO molecules) for 35 ps.

We evaluated the coverage dependence of the CO stretch frequency by calculating vibrational frequencies for CO adsorbed on solid Pt(111) and Pt(211) surfaces to obtain results for terrace and edge sites, respectively. On that account, super cells with varying size were generated for Pt(111), namely, a c(4 × 2) structure with one CO at an on-top and one CO at a bridge position (0.5 ML) to investigate high coverage, a ($\sqrt{3} \times \sqrt{3}$ R30°) cell with one CO adsorbed on-top (0.33 ML), and (4 × 4) as well as (5 × 5) geometries with CO adsorbed on-top for low coverage (0.0625 and 0.04 ML). For Pt(211) (1 × 2) and (2 × 4), super cells with CO adsorbed on-top of Pt edge atoms were generated to investigate high and low coverage, respectively. Slab models consisted of six layers of Pt, where three bottom layers were kept to the bulk geometry during geometry optimization while three surface layers were allowed to relax. The first Brillouin Zone was sampled using a 21 × 21 × 21 *k*-point mesh for the optimized bulk geometry with a lattice constant of 3.92 Å, and corresponding sizes were used for the super cells together with a Methfessel−Paxton-smearing of first order with a smearing parameter of σ = 0.2 eV.[36] For all geometry optimizations an energy converge criterion of 10^{-8} eV was chosen, and geometries were relaxed until the forces on all atoms were smaller than 0.01 and 0.001 eV/Å for surfaces with and without adsorbates, respectively. The cutoff for the plane wave basis was set to 480 eV. Furthermore, a polyhedral Pt_{201} NP was generated exhibiting large (111) and small (100) facets to compare experimental results for the pure Pt catalyst (see Figure S5). Here, on-top adsorption of CO was tested for edge, corner, and terrace Pt sites for (111) facets. Vibrational frequencies of the aforementioned geometries were computed using a finite differences approach by displacing all corresponding atoms by 0.01 Å in all spatial directions. The Bader approach was used to calculate atomic charges from an all-electron charge density.[37,38]

The influence of coadsorbates on the CO vibrational frequency was assessed using a solid model system, namely, a fcc-Ga(100) slab (computed bulk lattice constant: 4.18 Å) with an additional Pt atom adsorbed in surface hollow position in analogy to the isolated active Pt center in the liquid. Γ-including 25 × 25 × 25 and 8 × 8 × 1 *k*-point meshes were employed for the bulk and the (3 × 3 × 3) super cell containing 6 layers (three fixed to the bulk geometry and three free to relax). The remaining setup was chosen as described for the Pt(111) system. Subsequently, CO was adsorbed on top of the Pt surface atom together with different coadsorbates in its vicinity, namely, one or two H atoms as well as propane, propene, and a propyl residue. The corresponding structures are shown in the Supporting Information (Figure S6). Densities of states (DOS) were computed using an increased *k*-point mesh (26 × 26 × 1) in combination with the tetrahedron method with Blöchl corrections.[39]

3. RESULTS AND DISCUSSION

During the operando experiments, a total of five pulses carrying Ar/CO in propane were applied. The analysis showed that the GC and IR data are highly reproducible at each temperature step, which underlines the stability of the system and the accuracy of the automatized procedure. Hence, the figures presented in this section show IR spectra and conversion/selectivity values averaged over the five gas pulses. Concerning the IR spectra, only data recorded during the Ar-containing pulse are considered. As Figure 1 illustrates, GC pulses are averaged separately during dosing of Ar/propane and CO/propane, to investigate the influence of CO on the catalytic performance.

3.1. Characterization of the GaPt Catalyst by DFT.

Similar as in our previous work, we performed DFT calculations to obtain insight into the surface composition and Ga/Pt distribution.[9] Different models were investigated: a liquid slab model containing 178 Ga atoms and 2 Pt atoms, a pure Ga_{135} nanoparticle (NP), a $Ga_{132}Pt_3$ NP and a $Ga_{125}Pt_{10}$ NP (see section 2.4). In Figure S3 the densities of the pure Ga and the high-Pt-content $Ga_{125}Pt_{10}$ NPs are plotted as a function of the distance from the NP center. We observe similar effects as in our previous work, where only slab models were utilized to examine the catalyst structure. In particular, we find a layering of the two species for both types of NPs. Furthermore, Pt is depleted at the surface but shows an enhanced concentration in the subsurface region. Previously, we suggested that the Pt atoms are still able to reach the surface because of the high mobility in the liquid sample at elevated temperatures, where they act as single-atom

DOI: 10.1021/acscatal.8b04578
ACS Catal. 2019, 9, 2842−2853

catalytic centers. This effect is indeed observable in Figure 2, where the temporal evolution of the distance from the NP center

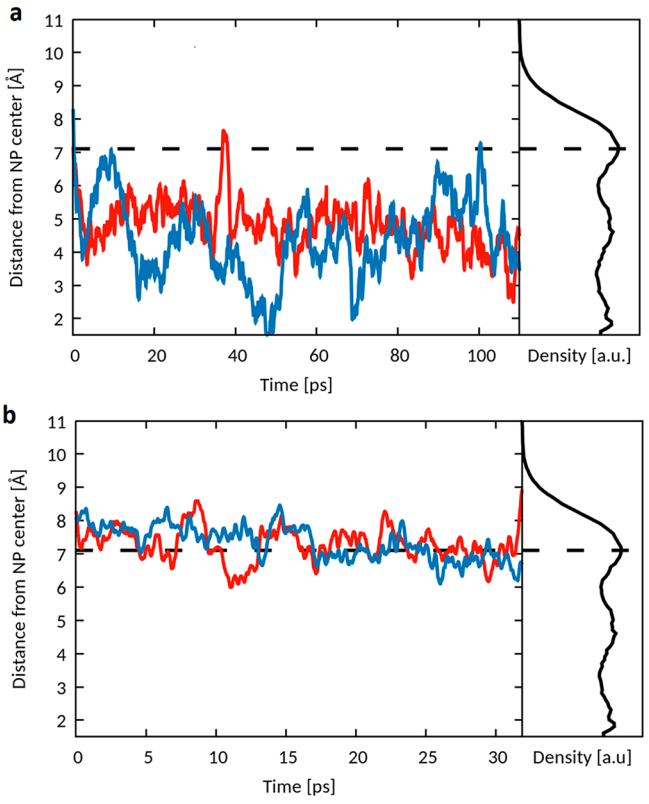

Figure 2. Distance from the NP center for two selected Pt atoms as a function of time as obtained in ab initio molecular dynamics (AIMD) simulations. The Pt atoms were initially located at the surface: (a) without adsorbed CO, (b) with adsorbed CO. The Ga density (a.u., arbitrary units) is plotted for comparison; the dashed line resembles the first maximum in the Ga density.

is plotted for two Pt atoms in $Ga_{132}Pt_3$ which were initially located at the surface. In the beginning of the simulation, the Pt atoms quickly leave the surface. However, as time evolves they emerge at the surface from time to time, available for approaching reactants. The same behavior is found for our slab model, where one Pt atom is initially located at each surface of the slab. Again, the Pt atoms leave the surface directly in the beginning of the AIMD run which reflects the tendency for surface depletion (Figure S4). The rate of appearance at the surface will depend on several factors, e.g., the size of the NP and the mobility of the atoms, which in turn depends on the temperature and the composition of the catalyst. When the temperature is higher, the mobility of the atoms is higher, and thus, the ability of Pt to reach the surface is higher. In addition, the residence time of Pt at the surface can be strongly influenced by adsorbates, as further described in the following section.

3.2. CO Adsorption on Pt/Al_2O_3 and $Ga_{37}Pt/Al_2O_3$. The position of the IR bands arising from the CO probe molecule depends on the noble metal sites available, on the CO coverage, and on electronic effects induced by coadsorbates.[40,41] To be able to identify the influence of hydrocarbons in the operando experiment, we first tested the adsorption of CO on Pt samples with and without Ga in the absence of propane.

Figure 3 shows the DRIFT spectra obtained after CO dosing and subsequent removal of the gas phase at 200, 300, and 400 °C on Pt/Al_2O_3 and $Ga_{37}Pt/Al_2O_3$. The Pt/Al_2O_3 sample shows a

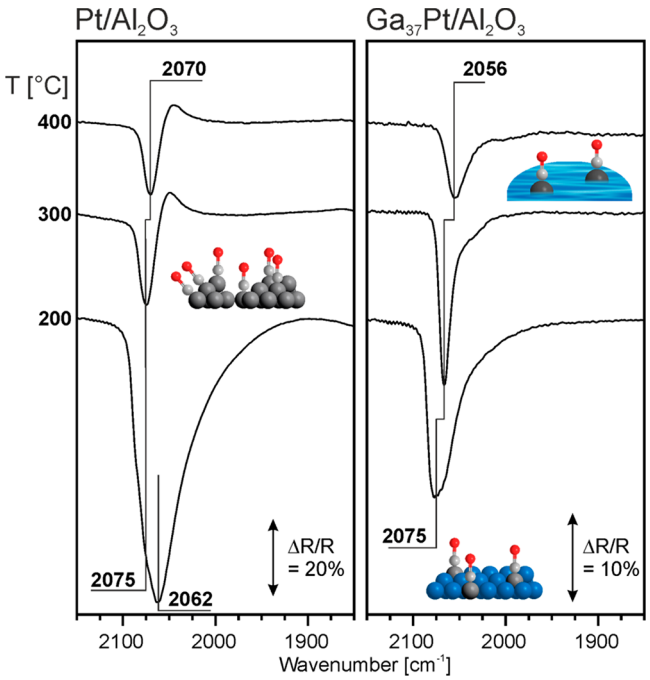

Figure 3. DRIFT spectra obtained during CO adsorption on two Pt-containing catalysts, namely, Pt/Al_2O_3 and $Ga_{37}Pt/Al_2O_3$.

pronounced peak at 2062 cm^{-1}. A shoulder at 2075 cm^{-1} can be seen at 200 °C. The signals can be attributed to on-top features on Pt, which shift to lower wavenumbers upon heating because of a decrease of the CO coverage.[40,42] As the coordination number of the Pt atom influences the exact position of the band, one can differentiate, for example, between Pt terraces and defect sites like steps, edges, or corners.[42,43] At temperatures above 200 °C differentiation between distinct sites is not possible.

The spectra obtained from $Ga_{37}Pt/Al_2O_3$ show a single peak at 2075 cm^{-1} that undergoes a constant shift to 2056 cm^{-1} upon heating. This shift can again be ascribed to coverage-related effects. Nevertheless, it should be stressed that the total area of the CO peak, which can serve as a measure for the CO coverage, is rather stable with increasing temperature, in contrast to the trend observed for Pt/Al_2O_3. This can be explained by CO coupling and mobility as described more thoroughly below. According to the Ga−Pt phase diagram, the 37:1 molar mixture of Ga and Pt melts at temperatures between 270 and 330 °C, i.e., within the temperature range of the experiment.[13,21]

We conducted DFT calculations for CO on different Pt systems, namely, Pt(111), Pt(211), and Pt_{201} NPs, to investigate the shifts of the vibrational frequencies of CO on terrace, edge, and defect sites. The results from DFT are summarized in Table 2 and compared to the experimental data from the literature to obtain a well-defined reference for our GaPt system.[44−46] Upon comparison of the data for Pt(111) and Pt(211), it is obvious that computed values for the CO stretching frequency underestimate the experimental findings for both surfaces. This is a well-described phenomenon for PBE-derived frequencies and can be corrected for by scaling factors depending on the system.[20,47−49] The data in Table 2 furthermore show that this scaling is not equal for all coverages, but rather dependent on the CO−CO distance. We observed a similar behavior for the CO adsorption on Pd(111) in our previous work.[15] While at higher coverage (0.5 ML) the

DOI: 10.1021/acscatal.8b04578
ACS Catal. 2019, 9, 2842−2853

Table 2. Comparison of Experimental and Calculated C−O Stretching Frequencies for Different Pt Systems

coverage	experimental frequency [cm^{-1}]	calculated frequency (shifted) [cm^{-1}]	difference [cm^{-1}]	CO−CO distance (DFT)
Pt(111),[a] ≥0.50 ML	2109−2110	2086 (2110)[c]	23−24	≤3.61
Pt(111),[a] 0.33 ML	2100	2079 (2103)	21	4.80
Pt(111),[a] ≤0.1 ML	2094−2096	2060−2062 (2094−2096)	34	≥8.75
Pt(211),[b] high	2077	2053 (2077)	24	5.54
Pt(211),[b] low	2071	2037 (2071)	34	11.08
Pt_{201}, corner		2022 (2056)		
Pt_{201}, edge		2029 (2063)		
Pt_{201}, terrace		2062 (2096)		

[a]Ref 44. [b]Refs 45 and 46. [c]Calculated at 0.5 ML.

calculated frequencies are only 21−24 cm^{-1} smaller than the experimental ones, the difference becomes larger at low coverage (34 cm^{-1}), both for Pt(111) and Pt(211). Hence, for smaller CO−CO distances the DFT-derived frequencies are shifted by 24 cm^{-1}, and for larger distances (>9 Å) by 34 cm^{-1}.

Additionally, we examined a Pt_{201} polyhedral NP ($d \sim 1.7$ nm) (see Figure S5) with large (111) and small (100) facets. Adsorption of one CO molecule on the (111) facet reveals that the size of the terrace is large enough to be comparable to the perfect (111) surface, as indicated by a vibrational frequency of 2096 cm^{-1} after shifting [Pt(111): ≤0.1 ML 2094−2096 cm^{-1}]. We further probed different adsorption sites, namely, edges and corners, with the aim to assign the experimentally measured signals. We obtained shifted CO stretching frequencies of 2096, 2063, and 2056 cm^{-1} for terrace, edge, and corner sites, respectively. According to Greenler et al., high-, intermediate-, and low-coordinated sites like terraces, steps, and corners lead to features at >2080, 2070, and 2060 cm^{-1}, respectively.[50] Accordingly, we may assign the band at ∼2062 cm^{-1} to Pt corner atoms and the high-frequency shoulder at 2070 cm^{-1} to edge sites.[22] This is in line with our theoretical prediction, because the difference between the calculated frequencies of the two sites (Δ = 7 cm^{-1}) is in close agreement with experiment (Δ = 8 cm^{-1}). Note however that only one single CO molecule is adsorbed in the theoretical model, while the experimental coverage is higher, and increasing CO−CO interactions cause a blue-shift of the frequencies. Additionally, the experimental situation is far more complex, and thus, it is likely that the two signals do not evolve exclusively from corner and edge sites but are a mixture of different sites on (111) and (100) facets from NPs with varying size.[51]

The results of our AIMD simulations at 450 °C for CO adsorption on Pt surrounded by liquid Ga at the surface and the liquid $Ga_{132}Pt_3$ nanodroplet are depicted in Figure 4. Independent of the model, both the surface and the NP show one peak for the CO stretching vibration at 2041 and 2040 cm^{-1}, respectively, in agreement with experiments. Because of the large distance between the CO molecules (>10 Å), the frequencies were shifted by 34 cm^{-1} in analogy to the Pt(111) and Pt(211) surfaces. Furthermore, we probed the temperature dependence of the vibration by simulating the CO−Pt−Ga slab at a lower temperature of 227 °C. Here, the mean square displacement as a function of time still indicates that the system is liquid (which is expected because of the low Pt concentration in the slab: 2 Pt in 178 Ga atoms). We obtained a vibrational frequency of 2051 cm^{-1} after shifting, suggesting that, in addition to coverage-related effects, the CO vibrational frequency also depends on temperature. This shift is one possible reason for the shifts of the band position observed in the experiments, even though the peak area remained almost unchanged. At large CO−CO separation, no coverage-related shift should be present, and the bands are further red-shifted because of temperature effects. Additionally, higher temperatures might lead to an enhanced mobility of the atoms in the liquid, which could be the reason for the Pt appearing at the surface more frequently. The latter effect would also give rise to an enhanced peak area. From the AIMD simulation it can be observed that the CO molecules are able to retain Pt at the surface. The situation is depicted in Figure 2b where the distance of Pt from the NP center is plotted as a function of time. In all cases, the CO molecule keeps the Pt atoms at the surface for the whole simulation time. Additionally, new Pt atoms can occur dynamically at the surface, thus further increasing the Pt surface concentration.

3.3. Pristine Al_2O_3. A pure Al_2O_3 sample was examined to evaluate the intrinsic activity of the reactor during the operando measurements. Even in the absence of catalytically active

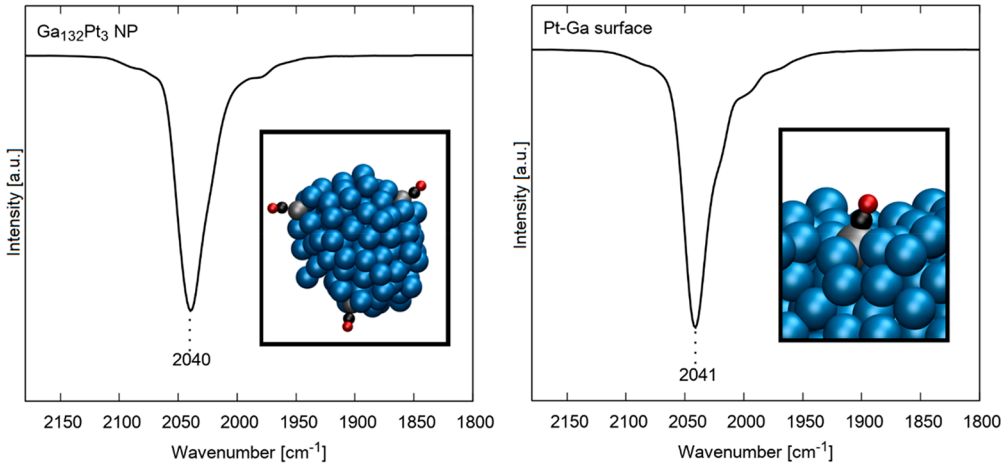

Figure 4. Vibrational spectra for the CO vibration on the $Ga_{132}Pt_3$ NP (left) and the slab model (right) calculated from the velocity−velocity autocorrelation function of AIMD simulations. Ga, Pt, C, and O are depicted in blue, silver, black, and red, respectively.

DOI: 10.1021/acscatal.8b04578
ACS Catal. 2019, 9, 2842−2853

material, we expect some cracking of propane on the stainless-steel reactor walls, especially at high temperatures. Moreover, hydrocarbon impurities in the propane gas feed like methane, ethane, or butane may affect the conversion data.

As shown in Figure 5, the nominal conversion does not reach values below 0.1%, mostly because of impurities in the gas feed.

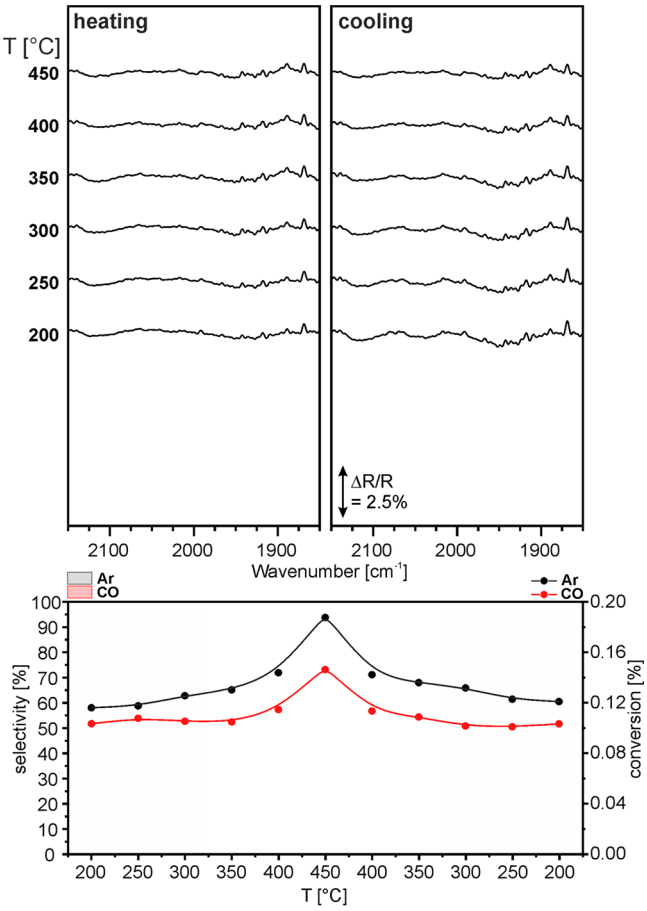

Figure 5. (top panel) Operando DRIFT spectra recorded on the Al_2O_3 sample at selected temperatures. (bottom panel) Conversion of propane for the Al_2O_3 sample.

At 450 °C values up to 0.18% are calculated mainly because of cracking at the hot reactor walls. The conversion is slightly higher during the propane pulses containing Ar than those containing CO.

The background activity depends on the experimental setup, procedure, and gas feed. To deal with the background activity, the data for the Ga_xPt_y/Al_2O_3 samples were corrected. To that aim, the integrated GC peak areas recorded in the blind experiment with Al_2O_3 were subtracted from the peak areas obtained for metal-containing samples. The procedure is illustrated in the Supporting Information in Figure S7.

In the DRIFT spectra depicted in Figure 5, no peaks are found in the CO region. This observation confirms that all peaks detected on the Ga_xPt_y/Al_2O_3 samples are due to adsorption of CO on metals.

3.4. Ga/Al_2O_3. Figure 6 depicts the carbonyl region obtained from the Ga/Al_2O_3 sample. No peaks are observed during the experiment. Evaluation of the GC data shows propane conversion above 350 °C, reaching ~1.1% at 450 °C with

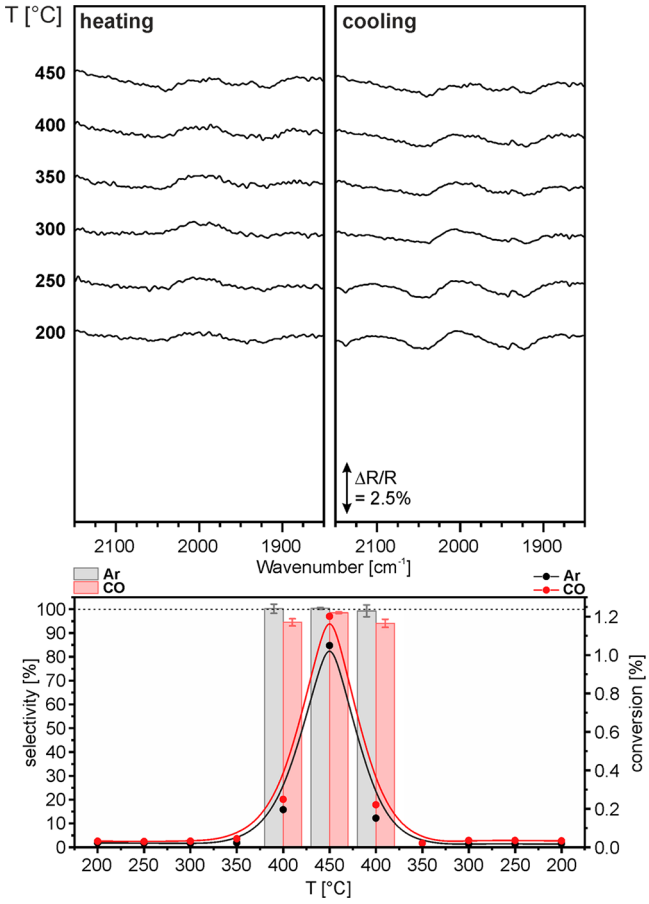

Figure 6. (top panel) Operando DRIFT spectra recorded on the Ga/Al_2O_3 sample at selected temperatures. (bottom panel) Conversion of propane and selectivity toward propene for the Ga/Al_2O_3 sample (lines are guides to the eye).

>90% selectivity toward propene. Conversion and selectivity are similar in the presence of CO and Ar.

The catalytic activity cannot be ascribed to the presence of fully metallic (reduced) Ga, as Ga^0 is known to be inactive toward dehydrogenation of alkanes.[6] Oxidic Ga^{3+}, however, is a well-known dehydrogenation catalyst and used for propane dehydrogenation, for example, in combination with Pt as a promoter.[5] It is assumed that tetrahedrally coordinated Ga^{3+} ions are the active sites for C−H activation in these dehydrogenation reactions.[3,5,6] Taking this into account, we attribute the catalytic activity observed to residual oxidic Ga, probably Ga^+ species.[52]

In the presence of noble metals full reduction is achieved, which can be explained by spillover of hydrogen species from the noble metal to the oxidic Ga.[53−55] Therefore, the catalytic activity of mixed Ga_xPt_y samples can solely be attributed to Pt species.

3.5. Pt/Al_2O_3. In Figure 7 we show the data obtained from the Pt/Al_2O_3 sample. A pronounced peak is present in the DRIFT spectra, which shifts from ~2050 to ~2000 cm^{-1} upon heating. This shift is reversed upon cooling. Interestingly, the CO feature is narrower after cooling back to 200 °C as compared to the beginning of the heating ramp.

Comparison of the spectra recorded at 200 °C after dosing of CO (section 3.2 and Figure 3) and of CO/propane (Figure 7) shows that the presence of propane leads to a red-shift of the CO band ($\Delta \approx 20$ cm^{-1}). The shift to lower wavenumbers may be

DOI: 10.1021/acscatal.8b04578
ACS Catal. 2019, 9, 2842−2853

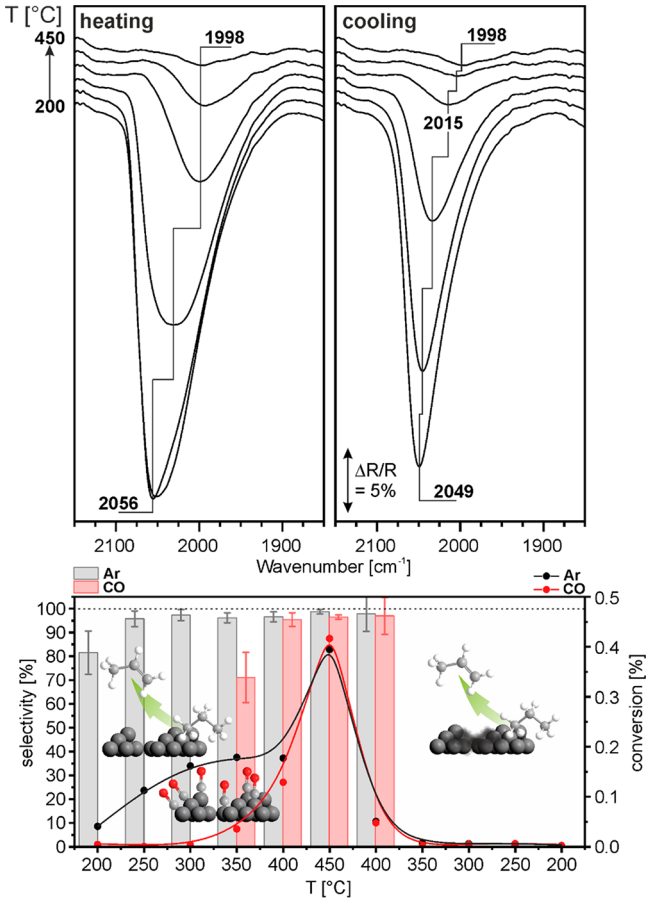

Figure 7. (top panel) Operando DRIFT spectra recorded on the Pt/Al_2O_3 sample at selected temperatures. (bottom panel) Conversion of propane and selectivity toward propene for the Pt/Al_2O_3 sample (lines are guides to the eye).

associated with the presence of σ-bound hydrocarbon coadsorbates, which leads to enhanced π-back-donation from the metal surface to the CO molecule.[56] On the basis of DFT calculations, this effect will be more thoroughly discussed for the GaPt example in the next section.

The GC data show a striking difference between the CO- and Ar-containing propane pulses. In Ar/propane, the conversion increases quickly from ~0.05% to ~0.2% by heating from 200 to 350 °C. Virtually no conversion is found for Pt/Al_2O_3 in CO/propane upon heating to 350 °C. At 400 °C the conversion increases, but it is still evident that the activity is higher in Ar. At 450 °C, a similar value of ~0.4% conversion is reached for both types of gas feeds with selectivity of >95%. Interestingly, similar behavior is found during cooling in Ar/propane and in CO/propane, respectively. Here, the conversion drops to values below 0.1% at 400 °C. In general, the trend during cooling resembles the behavior during heating in CO/propane.

The lower catalytic activity in the presence of CO upon heating the Pt/Al_2O_3 sample can be explained by CO poisoning. It is well-known that catalytically active sites on Pt are occupied because of the strong adsorption of CO, and thus, adsorption and conversion of hydrocarbons like propane or ethylene is hindered.[56,57] At temperatures below 400 °C during heating, some sites that lead to conversion of propane in Ar are blocked in the presence of CO. At 400 °C and above, Pt/Al_2O_3 is catalytically active even in the presence of CO. This observation indicates that CO is desorbed from the active Pt sites at these temperatures. The fact that the Pt/Al_2O_3 catalyst is poisoned upon cooling even in the absence of CO can be explained by carbon formation during the experiment.

Extensive studies on CO and carbon poisoning have been performed in the past to elucidate which sites are affected the most and to clarify the effects of selective poisoning on conversion and selectivity. It was reported that intermediate-coordinated Pt sites (steps, edges) and low-coordinated atoms (corners, apex atoms) are highly active for propane conversion, but also for dehydrogenation and the formation of cracking products.[7,58] Arteaga et al. showed that corner/apex atoms were resistant toward coking, but edge sites were heavily poisoned as they not only lead to hydrocarbon decomposition, but also provide suitable binding sites for adsorbed carbon.[59]

Following these arguments, we propose that initial conversion of propane during the Ar/propane pulses is due to reaction at Pt edges where carbon formation is likely to occur. This implies that a substantial amount of the most active Pt sites is selectively poisoned with carbon already at 400 °C during the heating ramp. Further conversion is expected to occur on the leftover sites (such as corner/apex sites) which are less affected by carbon formation. As a result, the conversion during cooling in Ar/propane is lower as compared to the heating ramp where the Pt edge sites were still available.

The smaller bandwidth of the on-top CO peak in the DRIFT spectra can also be explained by selective blocking of Pt sites. CO adsorption on a heavily coked catalyst, however, is known to give rise to smaller and red-shifted signals.[59] This is not found in the present experiment. Only a minor loss of band intensity is observed when comparing the spectra before and after the reaction procedure at 200 °C. Thus, we conclude that only a small amount of the total Pt surface is poisoned by carbon.

3.6. $Ga_{37}Pt_1/Al_2O_3$. Figure 8 depicts the DRIFT spectra obtained from the $Ga_{37}Pt/Al_2O_3$ sample and the corresponding conversion and selectivity data. The spectra show a single peak at 2049 cm^{-1} at the beginning of the experiment at 200 °C. Upon heating to 300 °C, a shift to lower wavenumbers (2032 cm^{-1}) is observed. Further heating leads to a shift to higher wavenumbers again and to the formation of a shoulder at 2071 cm^{-1}. During cooling, the peak center of the main contribution stays at 2046 cm^{-1} and the high-frequency shoulder at 2071 cm^{-1} decreases in intensity. The peak obtained after cooling to 200 °C is less intense as compared to the one obtained at the beginning of the experiment.

As discussed above, CO does not adsorb on the Al_2O_3 support and on the reduced Ga phase. Furthermore, Ga hydride peaks were not detected under our experimental conditions, which would be expected to appear in the 1980–2020 cm^{-1} range.[60] Thus, the peaks observed in the spectra originate from Pt species in the Ga matrix exclusively and can be attributed to on-top bound CO.

In contrast to the Pt/Al_2O_3 sample, conversion and selectivity show the same trend in Ar- and CO-containing propane pulses in the case of $Ga_{37}Pt/Al_2O_3$. No conversion is observed below 350 °C. At 350 °C and above, a steep increase in activity is observed, with a maximum of 3.7% propane conversion at 450 °C. High selectivity toward propene is observed at temperatures above 350 °C. The selectivity at 450 °C (~90%) is slightly smaller compared to the values obtained at 400 °C (~95%). Conversion and selectivity show the same trend during the heating and cooling ramp.

According to the Ga–Pt phase diagram, the 37:1 molar mixture melts at temperatures between 270 and 330 °C.[13,21] The

DOI: 10.1021/acscatal.8b04578
ACS Catal. 2019, 9, 2842–2853

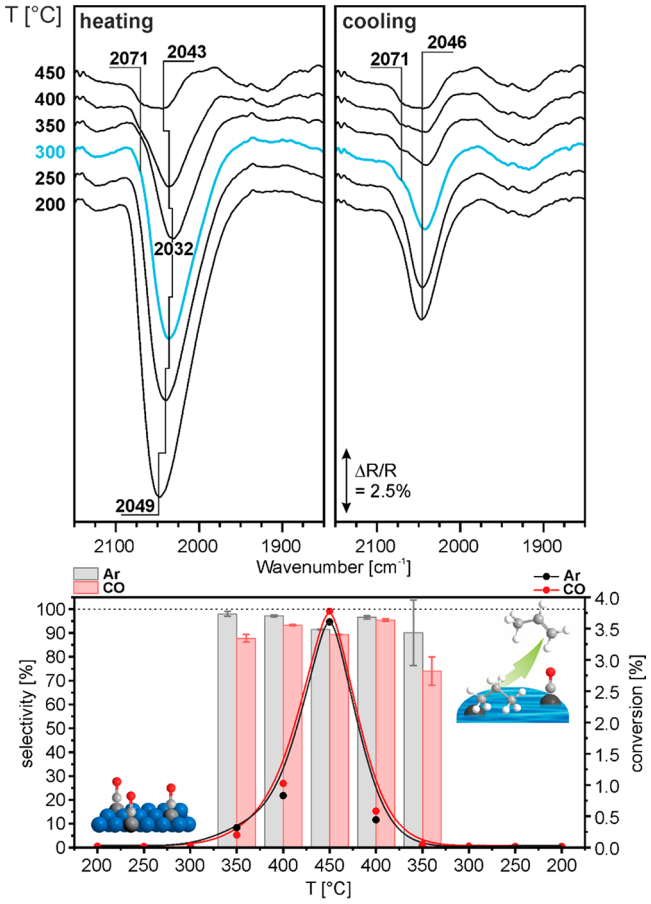

Figure 8. (top panel) Operando DRIFT spectra recorded on the $Ga_{37}Pt_1/Al_2O_3$ SCALMS sample at selected temperatures. (bottom panel) Conversion of propane and selectivity toward propene for the $Ga_{37}Pt_1/Al_2O_3$ SCALMS sample (lines are guides to the eye).

expected melting temperature matches the onset of the steep increase in conversion. We emphasize that, at temperatures above 350 °C, where the $Ga_{37}Pt$ mixture is clearly in the liquid state and shows the highest propane conversion, we still observe clear CO peaks in the DRIFT spectra. As Figure 8 shows, the catalytic performance of the $G_{37}Pt/Al_2O_3$ sample is not changed by the presence of CO as compared to the Ar-containing pulses, which in consequence means that the SCALMS system is not affected by CO poisoning. The fact that we observe CO adsorbates at temperatures where the $Ga_{37}Pt$ mixture is liquid, catalytically active, and shows no signs of CO poisoning suggests that the Pt species probed by CO are indeed the catalytically active sites in the SCALMS.

The blue-shift of the CO band observed upon heating from 300 to 450 °C indicates that the environment of the Pt sites is different from the conventional Pt catalyst, where a shift to lower wavenumbers is observed.[61] It is noteworthy that the behavior is also in contrast to what is observed on the same SCALMS in pure CO (see section 3.2 and Figure 3). We conclude that the blue-shift and the appearance of the high-frequency shoulder are associated not only with the formation of the liquid metal solution, but also with the presence of propane.

The spectra point to the coexistence of GaPt aggregates in a slightly different chemical and/or electronic environment, as there are at least two sites visible giving rise to the bands at 2071 and 2046 cm^{-1}, respectively. A possible explanation would be associated with the presence of GaPt droplets with different sizes and metal ratios. This explanation is unlikely, however, as we observe only a single peak in the experiments without propane. DFT calculations showed that C−H bond breaking of propane on noble metal atoms at the surface of the SCALMS is followed by diffusion of the residual hydrocarbon species onto the Ga matrix. The hydride species remain adsorbed at the noble metal sites where they can recombine and, finally, desorb as H_2. We assume that these reactive species may affect the charge distribution and, thereby, may also induce shifts of the CO band.

To explore such effects in more detail, we have performed DFT calculations on model systems. A fcc-Ga(100) surface model with one additional Pt atom at the surface was generated to simulate an isolated Pt site at a SCALMS interface. The calculated charge for Pt in the solid state (without CO, −0.88 e; with CO, −0.65 e) compares very well with the charge of the isolated Pt in the liquid SCALMS [without CO, −1.00 e (slab), −1.06 e (NP); with CO, −0.68 e (slab), −0.68 e (NP)], thus validating our solid surface model. Note that the charge on Pt without adsorbed CO is slightly higher in the liquid model,[62] because the Pt does not remain at the surface but is completely surrounded by Ga, while in the solid model system Pt is always located at the surface and thus less coordinated. Furthermore, CO adsorption at the surface Pt atom yields a CO vibrational frequency of 2034 cm^{-1}, which is in good comparison to the value computed for the liquid systems at 450 °C (~2040 cm^{-1}).

To understand the peak shifts during the conversion of propane, we study the effect of different coadsorbates on the CO stretching vibration, namely, propane, propene, a propyl residue, and atomic hydrogen. The corresponding adsorption geometries are shown in the Supporting Information (Figure S6); the vibrational frequencies of CO and charges of participating species are listed in Table 3. Upon adsorption of the

Table 3. Shifted CO Vibrational Frequencies and Bader Charges of Corresponding Species for CO Adsorption with Different Coadsorbates

coadsorbate	vibrational frequency [cm^{-1}]	charge Pt [e]	charge CO [e]	charge coadsorbate [e]
	2034	−0.65	−0.14	
1 H	2038	−0.55	−0.09	−0.13/H
2 H	2056	−0.43	−0.07	−0.14/H
propan	2029	−0.65	−0.14	−0.04
propen	2023	−0.65	−0.16	−0.01
propyl	2023	−0.71	−0.12	−0.28

hydrocarbons, the vibrational frequency is shifted to lower wavenumbers. This effect is in qualitative agreement with the experiment. An explanation can be derived from the bonding mechanism of CO to the Pt atom, in the framework of the Blyholder model[62] and the density of states (DOS). In Figure 9, the orbital-resolved DOS of the Pt atom and the CO molecule are depicted before (upper half) and after (lower half) adsorption. According to the Blyholder model, adsorption involves two contributions, namely, electron donation from the CO 5σ orbital to the metal and back-donation from the metal to the CO 2π* orbital. The latter weakens the CO bond and causes the red-shift upon adsorption.[62−64] The scenario is reflected by the changes in the DOS before and after CO adsorption for the case of Pt in Ga. Upon adsorption of CO, the peaks between −11 and −7 eV can be attributed to the interaction between d_z^2 and d_{xz}/d_{yz} states of the surface and the 4σ, 5σ, and 1π states of CO, respectively. In the regime from −5 eV to the Fermi level, the d

DOI: 10.1021/acscatal.8b04578
ACS Catal. 2019, 9, 2842−2853

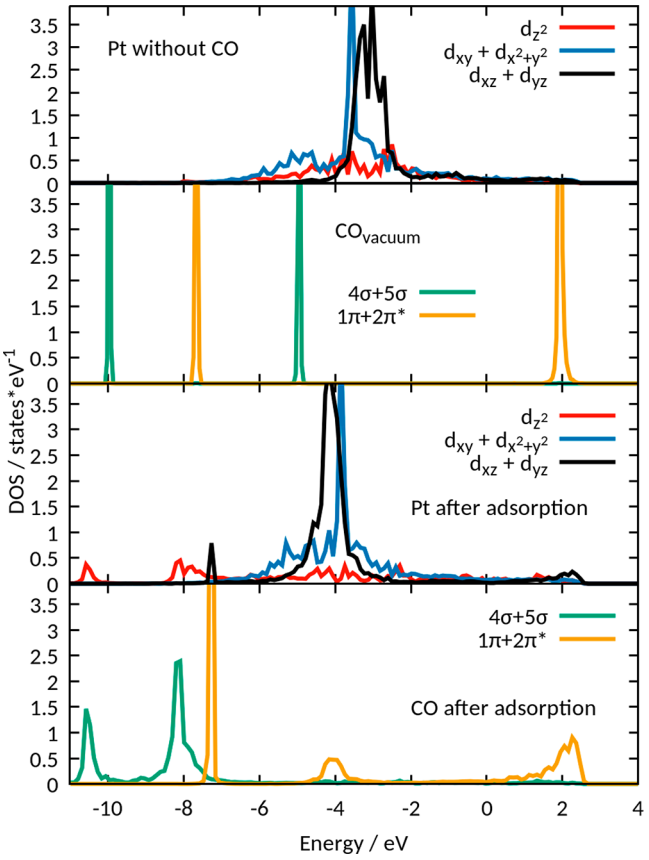

Figure 9. Orbital-resolved electronic density of states (DOS) on Pt model systems before and after adsorption of CO (see text for details).

contribution from the Pt dominates, and one additional contribution emerges (around −4 eV), which belongs to a hybrid of 1π and 2π* states of the CO molecule. As this state now lies below the Fermi level, it is occupied and filled by back-donated electrons.[63] The last region above the Fermi level consists of an antibonding hybrid orbital originating from the molecular 2π* and the d_{xz}/d_{yz} orbitals of the Pt atom. On the basis of this model, we can explain the red-shift upon coadsorption of the hydrocarbons. In fact, their coadsorption leads to increased back-donation from Pt to CO which, in turn, weakens the CO bond. In contrast, coadsorption of atomic hydrogen at the Pt center reduces the negative charge on Pt and, in turn, weakens back-donation and leads to a blue-shift. Thus, the DFT results are in good agreement with the experimental behavior. In general, the CO band is found to be shifted to lower wavenumbers because of the presence of hydrocarbons on the surface. We assume that the same effect can be observed on the pure Pt surface. It is noteworthy that previous studies have shown that, in addition to hydrocarbon coadsorption, hydrogen coadsorption on Pt(111) also weakens the CO bond and leads to a red-shift of the CO frequency.[65−67] This is in sharp contrast to the GaPt system where a blue-shift is observed upon hydrogen coadsorption both in experiment and calculation. This difference is caused by the difference in the charge distribution in the GaPt system. Our calculations show that the already negatively charged isolated Pt atom transfers charge to the H adsorbate upon adsorption (∼0.1−0.2 e per H; see Table 3). This reduces the charge at the Pt center which results in a lower back-donation to the CO and thus a blue-shift of the frequency.

The decrease of frequency upon heating to 300 °C can be related to the decreasing coverage and, hence, decreased CO−CO coupling and interaction. Subsequently, the band position shows a shift to higher wavenumbers again, and the shoulder at 2071 cm^{-1} emerges. We attribute these contributions to changes in the concentration of the different coadsorbates, according to the discussion above. The findings show that by vibrational spectroscopy of adsorbed CO we are able to probe the different chemical and electronic environments as a function of temperature, composition, and coadsorbates on the surface of liquid $Ga_{37}Pt$ droplets.

4. CONCLUSION

In the present study, we show that the active surface sites of a SCALMS can be probed under operando conditions by DRIFTS using CO as a probe molecule. Online GC is used to record the activity both in the absence and in the presence of CO. DFT is used as a tool to identify the nature of the active surface site and its spectroscopic properties. We compare the DRIFT spectra, activity, and selectivity of Al_2O_3, Pt/Al_2O_3, Ga/Al_2O_3, and $Ga_{37}Pt/Al_2O_3$ catalysts using identical fully automatized experimental procedures to ensure comparability of the data. The main conclusions can be summarized as follows:

(1) On the Ga/Al_2O_3 sample, Ga^+ species reside on the surface after reduction. These residual species are active for the conversion of propane and give rise to conversion of propane in the absence of noble metals. The Ga/Al_2O_3 sample is more active than Pt/Al_2O_3.

(2) Small Pt aggregates on the Pt/Al_2O_3 sample expose mainly intermediate- and low-coordinated Pt sites. These sites are active toward propane dehydrogenation at temperatures even below 300 °C. However, their activity is reduced by the presence of CO and through carbon poisoning. In particular, intermediate-coordinated Pt atoms on edge sites are prone to rapid accumulation of coke.

(3) The SCALMS catalyst $Ga_{37}Pt/Al_2O_3$ explored in this study showed the highest activity of the samples studied, combined with high selectivity to propene (>90%). We attribute the catalytic activity to isolated Pt atoms in the Ga matrix. The theoretical results show that Pt is depleted at the surface, but dynamically reappears at the surface. By adsorption, the Pt atoms can be retained at the surface. Different SCALMS nanoparticle models were tested in DFT and were shown to yield similar results as the slab models.

(4) Using CO as a probe molecule, we demonstrate that it is possible to monitor the active Pt sites under operando conditions without affecting the catalytic performance. Thus, the IR spectra represent the first operando DRIFT spectra of a catalytically active SCALMS system. We identify clear differences in the CO adsorption behavior as compared to the pure Pt catalyst. Specifically, we observe characteristic shifts of CO on isolated Pt sites. The bonding mechanism was investigated by DFT calculations, suggesting that the IR band shifts can be attributed to the presence of hydrocarbon coadsorbates on the Pt−Ga SCALMS. Comparison of the DOS before and after CO and hydrocarbon coadsorption suggests that the band shifts can be qualitatively rationalized on the basis of the Blyholder model. Expectedly, the Pt center in the $Ga_{37}Pt$ mixture shows different electronic features with respect to

DOI: 10.1021/acscatal.8b04578
ACS Catal. 2019, 9, 2842−2853

the pure Pt catalyst, as shown by the shift of the CO signal in the presence of hydrogen coadsorbates.

Reactor experiments that examine the catalytic performance of similar SCALMS systems in terms of activity, conversion, and selectivity at temperatures above 450 °C are being performed currently and will be reported in a future publication.

■ ASSOCIATED CONTENT

Supporting Information

The Supporting Information is available free of charge on the ACS Publications website at DOI: 10.1021/acscatal.8b04578.

Schematic representation of the operando IR setup, post-data-treatment to subtract gas-phase signals, supporting DFT results, analysis of experimental error in GC measurements, GC peak area correction, and SEM/EDX characterization (PDF)

■ AUTHOR INFORMATION

Corresponding Author

*E-mail: joerg.libuda@fau.de.

ORCID

Tanja Bauer: 0000-0002-6399-2954
Peter Wasserscheid: 0000-0003-0413-9539
Adrian Bonivardi: 0000-0002-8575-675X
Andreas Görling: 0000-0002-1831-3318
Jörg Libuda: 0000-0003-4713-5941

Author Contributions

▽T.B. and S.M. share first authorship.

Notes

The authors declare no competing financial interest.

■ ACKNOWLEDGMENTS

This project was financially supported by the Excellence Cluster "Engineering of Advanced Materials" in the framework of the excellence initiative (Bridge Funding). T.B. gratefully acknowledges financial support from the "Fonds der Chemischen Industrie". N.T. and P.W. gratefully acknowledge funding through the ERC Advanced Investigator Grant 786475 to P.W. that is dedicated to the further exploration of "SCALMS" materials. In addition, we acknowledge additional travel support through the CONICET/BAYLAT. The authors thank Fabian Waidhas for providing SEM and EDX data.

■ REFERENCES

(1) Sattler, J. J. H. B.; Ruiz-Martinez, J.; Santillan-Jimenez, E.; Weckhuysen, B. M. Catalytic Dehydrogenation of Light Alkanes on Metals and Metal Oxides. *Chem. Rev.* **2014**, *114*, 10613−10653.

(2) Michorczyk, P.; Ogonowski, J. Simultaneous Propane Dehydrogenation and CO_2 Hydrogenation over CrO_x/SiO_2 Catalyst. *React. Kinet. Catal. Lett.* **2005**, *87*, 177−183.

(3) Im, J.; Choi, M. Physicochemical Stabilization of Pt against Sintering for a Dehydrogenation Catalyst with High Activity, Selectivity, and Durability. *ACS Catal.* **2016**, *6*, 2819−2826.

(4) Rodríguez, L.; Romero, D.; Rodríguez, D.; Sánchez, J.; Domínguez, F.; Arteaga, G. Dehydrogenation of n-Butane over Pd−Ga/Al_2O_3 Catalysts. *Appl. Catal., A* **2010**, *373*, 66−70.

(5) Sattler, J. J. H. B.; Gonzalez-Jimenez, I. D.; Luo, L.; Stears, B. A.; Malek, A.; Barton, D. G.; Kilos, B. A.; Kaminsky, M. P.; Verhoeven, T. W. G. M.; Koers, E. J.; Baldus, M.; Weckhuysen, B. M. Platinum-Promoted Ga/Al_2O_3 as Highly Active, Selective, and Stable Catalyst for the Dehydrogenation of Propane. *Angew. Chem., Int. Ed.* **2014**, *53*, 9251−9256.

(6) Searles, K.; Siddiqi, G.; Safonova, O. V.; Copéret, C. Silica-supported Isolated Gallium Sites as Highly Active, Selective and Stable Propane Dehydrogenation Catalysts. *Chem. Sci.* **2017**, *8*, 2661−2666.

(7) Zhu, J.; Yang, M.-L.; Yu, Y.; Zhu, Y.-A.; Sui, Z.-J.; Zhou, X.-G.; Holmen, A.; Chen, D. Size-Dependent Reaction Mechanism and Kinetics for Propane Dehydrogenation over Pt Catalysts. *ACS Catal.* **2015**, *5*, 6310−6319.

(8) Saerens, S.; Sabbe, M. K.; Galvita, V. V.; Redekop, E. A.; Reyniers, M.-F.; Marin, G. B. The Positive Role of Hydrogen on the Dehydrogenation of Propane on Pt(111). *ACS Catal.* **2017**, *7*, 7495−7508.

(9) Taccardi, N.; Grabau, M.; Debuschewitz, J.; Distaso, M.; Brandl, M.; Hock, R.; Maier, F.; Papp, C.; Erhard, J.; Neiss, C.; Peukert, W.; Görling, A.; Steinrück, H. P.; Wasserscheid, P. Gallium-rich Pd−Ga Phases as Supported Liquid Metal Catalysts. *Nat. Chem.* **2017**, *9*, 862−867.

(10) Görling, A.; Steinrück, H.-P.; Taccardi, N.; Wasserscheid, P.; Debuschewitz, J. Catalytically Active Compositions of Matter. Patent WO 2018036672 A1, 2018.

(11) Armbrüster, M.; Schlögl, R.; Grin, Y. Intermetallic Compounds in Heterogeneous Catalysis − a Quickly Developing Field. *Sci. Technol. Adv. Mater.* **2014**, *15*, No. 034803.

(12) Tillard, M.; Belin, C. The new Intermetallic Compound Ga_5Pt: Structure From a Twinned Crystal. *Intermetallics* **2011**, *19*, 518−525.

(13) Okamoto, H. Ga-Pt (Gallium-Platinum). *J. Phase Equilib. Diffus.* **2007**, *28*, 494−494.

(14) Anres, P.; Gaune-Escard, M.; Bros, J. P. Thermodynamics of the (Rh−Ga) System. *J. Alloys Compd.* **1998**, *265*, 201−208.

(15) Föttinger, K.; Rupprechter, G. In Situ Spectroscopy of Complex Surface Reactions on Supported Pd−Zn, Pd−Ga, and Pd(Pt)−Cu Nanoparticles. *Acc. Chem. Res.* **2014**, *47*, 3071−3079.

(16) Haghofer, A.; Ferri, D.; Föttinger, K.; Rupprechter, G. Who Is Doing the Job? Unraveling the Role of Ga_2O_3in Methanol Steam Reforming on Pd_2Ga/Ga_2O_3. *ACS Catal.* **2012**, *2*, 2305−2315.

(17) Marcinkowski, M. D.; Darby, M. T.; Liu, J.; Wimble, J. M.; Lucci, F. R.; Lee, S.; Michaelides, A.; Flytzani-Stephanopoulos, M.; Stamatakis, M.; Sykes, E. C. H. Pt/Cu Single-Atom Alloys as Coke-Resistant Catalysts for Efficient C−H Activation. *Nat. Chem.* **2018**, *10*, 325−332.

(18) Tew, M. W.; Emerich, H.; van Bokhoven, J. A. Formation and Characterization of PdZn Alloy: A Very Selective Catalyst for Alkyne Semihydrogenation. *J. Phys. Chem. C* **2011**, *115*, 8457−8465.

(19) Liu, J.; Lucci, F. R.; Yang, M.; Lee, S.; Marcinkowski, M. D.; Therrien, A. J.; Williams, C. T.; Sykes, E. C. H.; Flytzani-Stephanopoulos, M. Tackling CO Poisoning with Single-Atom Alloy Catalysts. *J. Am. Chem. Soc.* **2016**, *138*, 6396−6399.

(20) Kettner, M.; Maisel, S.; Stumm, C.; Schwarz, M.; Schuschke, C.; Görling, A.; Libuda, J. Pd-Ga Model SCALMS: Characterization and Stability of Pd Single Atom Sites. *J. Catal.* **2019**, *369*, 33−46.

(21) Li, M.; Li, C.; Wang, F.; Zhang, W. Thermodynamic Assessment of the Ga−Pt System. *Intermetallics* **2006**, *14*, 826−831.

(22) Kaftan, A.; Schönweiz, A.; Nikiforidis, I.; Hieringer, W.; Dyballa, K. M.; Franke, R.; Görling, A.; Libuda, J.; Wasserscheid, P.; Laurin, M.; Haumann, M. Supported Homogeneous Catalyst Makes its own Liquid Phase. *J. Catal.* **2015**, *321*, 32−38.

(23) Xu, T.; Schwarz, M.; Werner, K.; Mohr, S.; Amende, M.; Libuda, J. The Surface Structure Matters: Thermal Stability of Phthalic Acid Anchored to Atomically-Defined Cobalt Oxide Films. *Phys. Chem. Chem. Phys.* **2016**, *18*, 10419−10427.

(24) Shriver, D.; Shirk, A.; Dilts, J. Trihydrido (Trimethylamine) Gallium. *Inorg. Synth.* **2007**, *17*, 42−45.

(25) Cochran, C. N.; Foster, L. M. Vapor Pressure of Gallium, Stability of Gallium Suboxide Vapor, and Equilibria of Some Reactions Producing Gallium Suboxide Vapor. *J. Electrochem. Soc.* **1962**, *109*, 144−148.

(26) Kresse, G.; Furthmüller, J. Efficient Iterative Schemes for ab initio Total-Energy Calculations Using a Plane-Wave Basis Set. *Phys. Rev. B: Condens. Matter Mater. Phys.* **1996**, *54*, 11169−11186.

DOI: 10.1021/acscatal.8b04578
ACS Catal. 2019, 9, 2842−2853

(27) Kresse, G.; Furthmüller, J. Efficiency of ab-initio Total Energy Calculations for Metals and Semiconductors Using a Plane-Wave Basis Set. *Comput. Mater. Sci.* **1996**, *6*, 15−50.
(28) Kresse, G.; Joubert, D. From Ultrasoft Pseudopotentials to the Projector Augmented-Wave Method. *Phys. Rev. B: Condens. Matter Mater. Phys.* **1999**, *59*, 1758−1775.
(29) Perdew, J. P.; Burke, K.; Enzerhof, M. Generalized Gradient Approximation Made Simple. *Phys. Rev. Lett.* **1996**, *77*, 3865−3868.
(30) Grimme, S.; Antony, J.; Ehrlich, S.; Krieg, H. A Consistent and Accurate ab initio Parametrization of Density Functional Dispersion Correction (DFT-D) for the 94 Elements H-Pu. *J. Chem. Phys.* **2010**, *132*, 154104.
(31) Grabau, M.; Erhard, J.; Taccardi, N.; Calderon, S. K.; Wasserscheid, P.; Goerling, A.; Steinrueck, H.-P.; Papp, C. Spectroscopic Observation and Molecular Dynamics Simulation of Ga Surface Segregation in Liquid Pd-Ga Alloys. *Chem. - Eur. J.* **2017**, *23*, 17701−17706.
(32) Nosé, S. A Unified Formulation of the Constant Temperature Molecular Dynamics Methods. *J. Chem. Phys.* **1984**, *81*, 511−519.
(33) Mermin, N. D. Thermal Properties of the Inhomogeneous Electron Gas. *Phys. Rev.* **1965**, *137*, A1441−A1443.
(34) Brehm, M.; Kirchner, B. TRAVIS − A Free Analyzer and Visualizer for Monte Carlo and Molecular Dynamics Trajectories. *J. Chem. Inf. Model.* **2011**, *51*, 2007−2023.
(35) Thomas, M.; Brehm, M.; Kirchner, B. Voronoi Dipole Moments for the Simulation of Bulk Phase Vibrational Spectra. *Phys. Chem. Chem. Phys.* **2015**, *17*, 3207−3213.
(36) Methfessel, M.; Paxton, A. T. High-Precision Sampling for Brillouin-Zone Integration in Metals. *Phys. Rev. B: Condens. Matter Mater. Phys.* **1989**, *40*, 3616−3621.
(37) Tang, W.; Sanville, E.; Henkelman, G. A Grid-Based Bader Analysis Algorithm Without Lattice Bias. *J. Phys.: Condens. Matter* **2009**, *21*, No. 084204.
(38) Henkelman, G.; Arnaldsson, A.; Jónsson, H. A Fast and Robust Algorithm for Bader Decomposition of Charge Density. *Comput. Mater. Sci.* **2006**, *36*, 354−360.
(39) Blöchl, P. E.; Jepsen, O.; Andersen, O. K. Improved Tetrahedron Method for Brillouin-Zone Integrations. *Phys. Rev. B: Condens. Matter Mater. Phys.* **1994**, *49*, 16223−16233.
(40) Hoffmann, F. M. Infrared Reflection-Absorption Spectroscopy of Adsorbed Molecules. *Surf. Sci. Rep.* **1983**, *3*, 107−192.
(41) Mehl, S.; Bauer, T.; Brummel, O.; Pohako-Esko, K.; Schulz, P.; Wasserscheid, P.; Libuda, J. Ionic-Liquid-Modified Hybrid Materials Prepared by Physical Vapor Codeposition: Cobalt and Cobalt Oxide Nanoparticles in $[C_1C_2Im][OTf]$ Monitored by In Situ IR Spectroscopy. *Langmuir* **2016**, *32*, 8613−8622.
(42) Asokan, C.; DeRita, L.; Christopher, P. Using Probe Molecule FTIR Spectroscopy to Identify and Characterize Pt-Group Metal Based Single Atom Catalysts. *Chin. J. Catal.* **2017**, *38*, 1473−1480.
(43) Haneda, M.; Watanabe, T.; Kamiuchi, N.; Ozawa, M. Effect of Platinum Dispersion on the Catalytic Activity of Pt/Al2O3 for the Oxidation of Carbon Monoxide and Propene. *Appl. Catal., B* **2013**, *142−143*, 8−14.
(44) Heyden, B. E.; Bradshaw, A. M. The Adsorption of CO on Pt(111) Studied by Infrared Reflection-Absorption Spectroscopy. *Surf. Sci.* **1983**, *125*, 787−802.
(45) Creighan, S. C.; Mukerji, R. J.; Bolina, A. S.; Lewis, D. W.; Brown, W. A. The Adsorption of CO on the Stepped Pt(211) Surface: A Comparison of Theory and Experiment. *Catal. Lett.* **2003**, *88*, 39−45.
(46) Mukerji, R. J.; Bolina, A. S.; Brown, W. A. A RAIRS and TPD Investigation of the Adsorption of CO on Pt(211). *Surf. Sci.* **2003**, *527*, 198−208.
(47) Prinz, J.; Gaspari, R.; Stöckl, Q. S.; Gille, P.; Armbrüster, M.; Brune, H.; Gröning, O.; Pignedoli, C. A.; Passerone, D.; Widmer, R. Ensemble Effect Evidenced by CO Adsorption on the 3-Fold PdGa Surfaces. *J. Phys. Chem. C* **2014**, *118*, 12260−12265.
(48) Yudanov, I. V.; Sahnoun, R.; Neyman, K. M.; Rösch, N.; Hoffmann, J.; Schauermann, S.; Johánek, V.; Unterhalt, H.; Rupprechter, G.; Libuda, J.; Freund, H.-J. CO Adsorption on Pd Nanoparticles: Density Functional and Vibrational Spectroscopy Studies. *J. Phys. Chem. B* **2003**, *107*, 255−264.
(49) Merrick, J. P.; Moran, D.; Radom, L. An Evaluation of Harmonic Vibrational Frequency Scale Factors. *J. Phys. Chem. A* **2007**, *111*, 11683−11700.
(50) Greenler, R. G.; Brandt, R. K. The Origins of Multiple Bands in the Infrared Spectra of Carbon Monoxide Adsorbed on Metal Surfaces. *Colloids Surf., A* **1995**, *105*, 19−26.
(51) Lentz, C.; Jand, S. P.; Melke, J.; Roth, C.; Kaghazchi, P. DRIFTS Study of CO Adsorption on Pt Nanoparticles Supported by DFT Calculations. *J. Mol. Catal. A: Chem.* **2017**, *426*, 1−9.
(52) Collins, S. E.; Baltanás, M. A.; Garcia Fierro, J. L.; Bonivardi, A. L. Gallium-Hydrogen Bond Formation on Gallium and Gallium-Palladium Silica-Supported Catalysts. *J. Catal.* **2002**, *211*, 252−264.
(53) Haneda, M.; Joubert, E.; Menezo, J.-C.; Duprez, D.; Barbier, J.; Bion, N.; Daturi, M.; Saussey, J.; Lavalley, J.-C.; Hamada, H. Surface Characterization of Alumina-Supported Catalysts Prepared by Sol-Gel Method. Part II − Surface Reactivity with CO. *Phys. Chem. Chem. Phys.* **2001**, *3*, 1371−1375.
(54) Collins, S. E.; Chiavassa, D. L.; Bonivardi, A. L.; Baltanás, M. A. Hydrogen Spillover in Ga_2O_3-Pd/SiO_2 Catalysts for Methanol Synthesis from CO_2/H_2. *Catal. Lett.* **2005**, *103*, 83−88.
(55) Li, L.; Zhang, B.; Kunkes, E.; Föttinger, K.; Armbrüster, M.; Su, D. S.; Wei, W.; Schlögl, R.; Behrens, M. Ga-Pd/Ga_2O_3 Catalysts: The Role of Gallia Polymorphs, Intermetallic Compounds, and Pretreatment Conditions on Selectivity and Stability in Different Reactions. *ChemCatChem* **2012**, *4*, 1764−1775.
(56) Yang, M.; Rioux, R. M.; Somorjai, G. A. Reaction Kinetics and In Situ Sum Frequency Generation Surface Vibrational Spectroscopy Studies of Cycloalkene Hydrogenation/Dehydrogenation on Pt(111): Substituent Effects and CO Poisoning. *J. Catal.* **2006**, *237*, 255−266.
(57) Chen, P.; Kung, K. Y.; Shen, Y. R.; Somorjai, G. A. Sum Frequency Generation Spectroscopic Study of CO/Ethylene Coadsorption on the Pt(111) Surface and CO Poisoning of Catalytic Ethylene Hydrogenation. *Surf. Sci.* **2001**, *494*, 289−297.
(58) Yang, M.-L.; Zhu, Y.-A.; Fan, C.; Sui, Z.-J.; Chen, D.; Zhou, X.-G. DFT Study of Propane Dehydrogenation on Pt Catalyst: Effects of Step Sites. *Phys. Chem. Chem. Phys.* **2011**, *13*, 3257−3267.
(59) Arteaga, G. J.; Anderson, J. A.; Rochester, C. H. FTIR study of CO Adsorption on Coked Pt−Sn/Al_2O_3 Catalysts. *Catal. Lett.* **1999**, *58*, 189−194.
(60) Collins, S. E.; Baltanás, M. A.; Bonivardi, A. L. Hydrogen Chemisorption on Gallium Oxide Polymorphs. *Langmuir* **2005**, *21*, 962−970.
(61) Lundwall, M. J.; McClure, S. M.; Goodman, D. W. Probing Terrace and Step Sites on Pt Nanoparticles Using CO and Ethylene. *J. Phys. Chem. C* **2010**, *114*, 7904−7912.
(62) Blyholder, G. Molecular Orbital View of Chemisorbed Carbon Monoxide. *J. Phys. Chem.* **1964**, *68*, 2772−2777.
(63) Kresse, G.; Gil, A.; Sautet, P. Significance of Single-Electron Energies for the Description of CO on Pt(111). *Phys. Rev. B: Condens. Matter Mater. Phys.* **2003**, *68*, No. 073401.
(64) Hammer, B.; Morikawa, Y.; Nørskov, J. K. CO Chemisorption at Metal Surfaces and Overlayers. *Phys. Rev. Lett.* **1996**, *76*, 2141−2144.
(65) Benvenutti, E. V.; Franken, L.; Moro, C. C.; Davanzo, C. U. FTIR Study of Hydrogen and Carbon Monoxide Adsorption on Pt/TiO_2, Pt/ZrO_2, and Pt/Al_2O_3. *Langmuir* **1999**, *15*, 8140−8146.
(66) Paleček, D.; Tek, G.; Lan, J.; Iannuzzi, M.; Hamm, P. Characterization of the Platinum−Hydrogen Bond by Surface-Sensitive Time-Resolved Infrared Spectroscopy. *J. Phys. Chem. Lett.* **2018**, *9*, 1254−1259.
(67) Ferri, D.; Bürgi, T.; Baiker, A. Pt and Pt/Al_2O_3 Thin Films for Investigation of Catalytic Solid-Liquid Interfaces by ATR-IR Spectroscopy: CO Adsorption, H_2-Induced Reconstruction and Surface-Enhanced Absorption. *J. Phys. Chem. B* **2001**, *105*, 3187−3195.

DOI: 10.1021/acscatal.8b04578
ACS Catal. 2019, 9, 2842−2853